On the probabilistic particle simulation of an arcjet flow expansion

D. Petkow[a], G. Herdrich[b], M. Pfeiffer[b], A. Mirza[b], S. Fasoulas[b], M. Matsui[c], K. Komurasaki[d]

[a] ESA-ESTEC
2200AG, Noordwijk, Keplerlaan 1, The Netherlands

[b] Universität Stuttgart
70569 Stuttgart, Pfaffenwaldring 31, Germany

[c] Shizuoka University
836 Ohya, Suruga-ku, Shizuoka-Shi, Shizuoka-Ken, 422-8529, Japan

[d] The University of Tokyo
7-3-1 Hongo, Bunkyo, Tokyo 113-8656, Japan

ABSTRACT

We apply a particle code (Direct Simulation Monte Carlo, DSMC) to a nozzle flow expansion set-up which is typical for thermal plasma spray systems. Although those systems tend to have a pressure level which is too high to be treated with DSMC we obtain good results with respect to Pitot pressure measurement based Mach number estimations at different axial distances from the nozzle exit plane. Precisely, we compare the Mach numbers at 0, 30, 60, and 90 mm distance from the nozzle exit plane which was chosen as inflow boundary. The relative deviation of the simulated Ma numbers from the measured is mostly about 10 %. An influence of the flow field upstream due to a static boundary condition downstream is also observed. The vital code extensions which allowed this simulation with DSMC are briefly discussed. Further code extensions for future research activities are outlined.

Keywords: DSMC, Particle simulation, Vacuum spraying, Arcjet facility, Nozzle expansion flow

1. Introduction

A variety of plasma-driven facilities is in use in order to reproduce the thermo-chemical loads experienced by a heat shield material during the atmospheric entry of a spacecraft [1]. Besides application fields like validation and improvement of models and codes, qualification of heat shield systems and development of aerothermodynamic measurement systems, there is also the scope of basic investigations e.g. oriented towards plasma-wall interaction. Here, the focus is often put on single gas investigations such as pure oxygen or oxygen / argon in order of being able to assess gas-specific test conditions e.g. to investigate catalysis [2].

Particle codes are used for the numerical investigation of rarefied as well as for dense flows. A two-dimensional DSMC particle code named LasVegas (see e.g. [3]) has been described and applied to a *rarefied* Argon nozzle expansion flow into a vacuum chamber [4]. Later, we applied the same code to *dense* arcjet flow conditions discussed in this work and in [5]. We use the term *dense flow* as an equivalent to *low Knudsen number flow* in order to avoid excessive discussions of the relation between the Knudsen number and appropriate numerical tools: Dense flows are commonly subject to continuum methods (Euler, Navier-Stokes), rarefied flows in many cases are subject to probabilistic particle methods like DSMC. For details please refer to [6].

Due to some limitations with respect to general

code features LasVegas failed to perform the simulation although Bird's DS2V code didn't, see [5]. Consequently, we extended LasVegas in order to provide the capability to simulate dense flows with DSMC. In detail, the spatial resolution is limited on basis of a minimum cell particle number and a nearest neighbor approach for the identification of the closest possible collision partner in a cell was implemented. Given that, dense flows can generally be treated with LasVegas. The same code is again applied to the arcjet facility operated by the University of Tokyo. Section 2 describes this arcjet in detail and also provides information on the measurement methodology. Section 3 gives a brief introduction to the applied numerical schemes and highlights the inflow conditions which were reconstructed from experimental measurements. Relevant code extensions enabling the arccjet simulation are described. The numerical results in comparison with the experimental measurements are discussed in Section 4. We conclude on the work done and on future activities in section 5.

2. Experimental procedure

The arcjet-driven plasma facility of the University of Tokyo was used to establish a test condition using Argon and Oxygen. The condition is shown in Table 1.

The facility itself consists of a thermal arcjet in the 1 kW power class and a vacuum chamber that has a diameter of roughly 80 cm and a length of about 1 m. In addition, there are a corresponding power supply and a vacuum pumping system as peripheral systems.

2.1 Arcjet plasma generator

An extensive description of the used thermal arcjet plasma generator, see Fig. 1, is given in [7].

Table 1 Operational conditions of facility.

Parameter	Values
Electrical power, P_{el}	1kW (U = 25V, I = 40A)
Total pressure, p_{0dc}	417 hPa
Ambient pressure, p_{amb}	20 Pa
Thermal efficiency, η_{Th}	47%
Mass flow rate (Ar)	0.12 g/s (4 slm)
Mass flow rate (O)	2.39 mg/s (0.1 slm)
Total mass flow rate	0.1224 g/s (4.1 slm)
Bulk enthalpy, h_{0eff}	3.9 MJ/kg

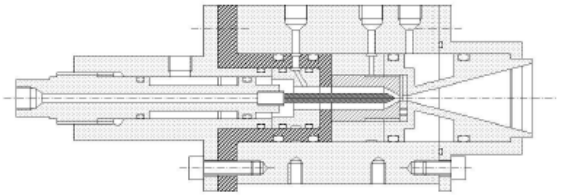

Fig. 1. Schematic of the thermal arcjet.

For the monitoring of the operational behavior of the device current and voltage (and, hence, power P_0), cooling temperatures, mass flow of the cooling water and plenum pressure p_0 are measured. In addition, the ambient pressure p_{amb} in the vacuum chamber and the working gas mass flow rates are measured as well. Correspondingly thermal efficiency η_{Th}, plasma power P_{Pl} and the bulk enthalpy h_{0eff} can be derived from the measured parameter, see [5]. Exemplarily, the bulk enthalpy is 3.90 MJ/kg, see also Table 1.

2.2 Mini pitot probe

The major motivation for a Mini Pitot probe for the measurement is the total pressure and correlated parameters such as Mach numbers.

Figure 2 shows the so-called Mini Pitot Pressure Probe of IRS which has been used for the arcjet campaigns at Tokyo University. The geometries [5] are of importance for both the overall integration in the facility and the correct interpretation of the data. The probe was used for the investigation of the flow field resulting from the test condition outlined in Table 1. Therefore, the positions x and y of the Pitot probe in the vacuum chamber was measured, too. The position x is the distance of the Pitot pressure bore from the nozzle exit plane of the plasma generator and y is the radial distance from the plasma jet centre i.e. the plasma generator axis.

Figure 2 depicts the used probe and its geometries (left) and the probe as mounted in the facility during a test. Clearly, the bow shock can be observed in the photograph on the right side of Fig. 2. Hence, the corresponding Mach numbers usually are above 1.

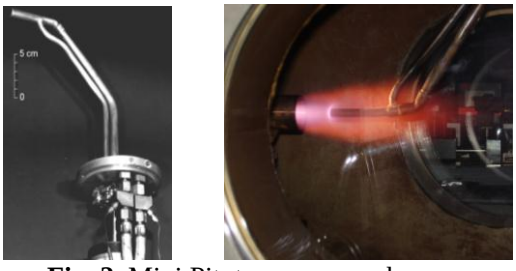

Fig. 2. Mini Pitot pressure probe.

During the experiments the resulting total pressure p_{tot} is detected using an adequate pressure gage. Using the pressure as such and assuming that the ambient pressure represents the static pressure in at the location of measurement proper Mach number equations can be provided:

$$Ma_1^{2\gamma} - C\gamma\left(\frac{p_{tot,2}}{p_1}\right)^{(\gamma-1)} Ma_1^2 + C\frac{(\gamma-1)}{2}\left(\frac{p_{tot,2}}{p_1}\right)^{(\gamma-1)} = 0 \quad (1)$$

This is the so-called Rayleigh-Pitot-Equation with $C = (2/(\gamma+1))^{(\gamma+1)}$ and is valid for super sonic conditions. The subscript 1 is related to the state before the shock, which is, therefore, in case of p the ambient pressure p_{amb}, and subscript 2 designates parameters behind the shock. The parameter γ is the ratio of the specific heats. However, from the plenum pressure and the ambient pressure it can be derived that the expected conditions are super-sonic. The maximum uncertainty for the Mach number due to the uncertainty of γ is 7 %, see e.g. [8].

3. Numerical method

In DSMC each simulated particle represents a number of real particles. Depending on the physical problem this number (macro particle factor) can reach 10^{16} or even more although an increase of that number causes statistical scattering in the results. Here, on needs to find a balance between accuracy, computational resources and simulation time.

One basic property of DSMC is the separation of movement and collision of the simulated particles. Both processes are treated subsequently. For the movement the classic equations of motion are solved. The critical modeling concerns generally the collision process which is treated probabilistically. This reduces the computational demand to a linear dependency on the particle number N which allows the simulation of technical problems. In each cell random pairs are collisionally evaluated. Exemplarily, if the cell contains 100 particles 50 pairs are generated and tested with respect to potential interactions. For comparison, in deterministic (i.e. molecular dynamics) simulations each particle interacts with every other particle in the cell which leads to an N^2 dependency.

The separation of collision and movement is realized by a time step size smaller than the inverse of the minimal collision frequency. For the discussed arcjet flow, we choose a time step size $\Delta t = 5 \cdot 10^{-9}$ s. For technical problems (i.e. on large geometric scales) that time step size is already very small. This is the reason why DSMC is commonly not applied to high density flows.

Each simulated particle represents $5 \cdot 10^{12}$ real particles. Total iteration number is $1.4 \cdot 10^5$.

For collisions we apply a standard (Variable Hard Sphere) model in which the energy dependent collision cross section is derived from viscosity data.

3.1 Domain and boundary conditions

The unstructured grid is generated making use of a self-developed Advancing Front algorithm with graphical user interface [9]. The computational domain is a rectangle with a width of 75 mm and a length of 250 mm. For the limits of this area five boundary conditions have been implemented. The upper line and on the right side of the rectangle are open with the ambient pressure impressed while the lower line is the symmetric axis of the flow. On the left side of the area an adiabatic wall is implemented. The left side lower corner is the center of the nozzle exit plane. Tank state can easily be estimated making use of the ideal gas equation: T = 300 K, v = 0 m/s, $n = 4.83 \cdot 10^{21}$ m^{-3} [5].

3.2 Inflow conditions

The initial mole fractions were estimated on basis of equilibrium assumptions in the discharge chamber. Therefore, we applied an equilibrium code (which is described in [10]) and used the input data given in Table 1. The resulting mole fractions are 95.10 % for Argon and 4.85 % for atomic Oxygen. Assuming a chemically frozen flow inside the nozzle we apply these mole fractions at the nozzle exit plane.

Using the Rayleigh-Pitot equation (1) the measured total pressure $p_{0e}(r)$ at the nozzle plane leads to a Mach number distribution $Ma_e(r)$, see Fig. 3.

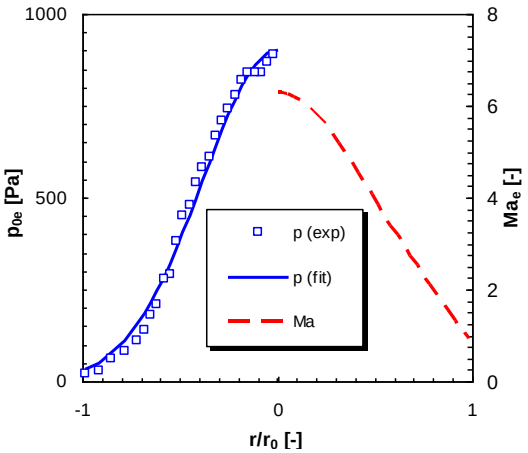

Fig. 3. Profiles for inflow condition at nozzle exit plane.

Despite frozen mole fractions we allow different adiabatic coefficients such that we average the Mach numbers over $1.1<\gamma<1.4$, for details see [8]. According to the free stream theory we assume a static pressure equal to the ambient tank pressure. Figure 3 shows exemplarily the experimental data as well as a deduced fit function.

Given these values we derived further quantities like the enthalpy distribution as well as temperature, particle density, and velocity profiles at the nozzle exit plane. For details of the modelling please refer to [5].

3.3 Code extensions

Previous attempts to simulated dense nozzle expansion flows with LasVegas [5] failed due to an unlimited spatial refinement: Grid adaptation was ruled only by the resolution criterion for the mean free path which needs to be resolved in each cell. Consequently, at high densities the cell number exploded which is equivalent to a thermal isolation of the particles. To avoid this we implemented a limit with respect to a minimum particle number in the cells.

Additionally, we implemented several algorithms which search for the closest collision partners in a cell. For the simulation was applied the standard nearest neighbor approach for N <= 50. Grid refinement is made if more than 50 particles are in the cell as a larger particle number quickly increases the computational load.

Given that, we merge both implementations (particle based limitation of grid cell adaptation and nearest neighbor search) in an advantageous way.

4. Result and discussion

Figure 4 depicts the comparison of the radial Mach number profiles at different axial distances from the nozzle exit plane (x = 0 mm). The x-axis in Fig. 4 is limited to the radius of the nozzle exit plane (r_0) since with increasing axial distance from the nozzle the radial velocity component increases which makes of Eq. (1) less applicable.

Not surprisingly, the reproduction of the Mach number profile at x = 0 mm is good although one observes a slight overestimation of the measured Mach numbers. At x = 30 mm the comparison between simulation and measurement is still good. With increasing distance from the center line measured Mach numbers seem to decrease faster than in the simulation. For x = 60 mm we observe a strong deviation between simulation and experiment.

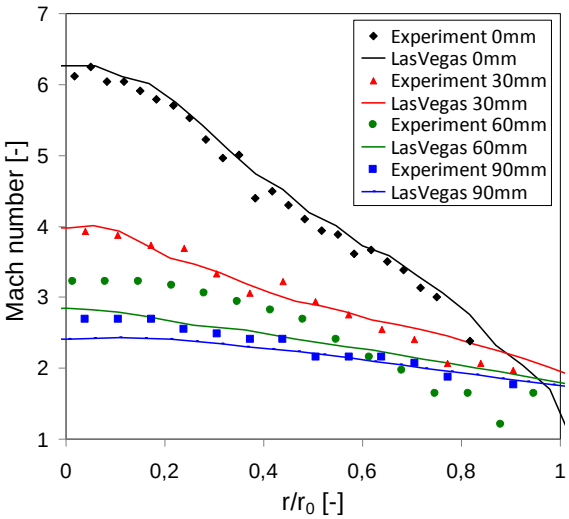

Fig. 4. Measured and simulated Mach number profiles.

For small radii, the measured values are underestimated, for large radii, Mach numbers are numerically overestimated. The match appears to be at $r/r_0 = 0.6$. With increasing axial distance (x = 90 mm) the agreement gets better again. In fact, at larger radii the matching appears to be better than at smaller radii. In total, we qualitatively reproduce the radial Mach number profiles at different axial distances from the nozzle exit plane.

Also, statistical scattering is observable which is inherent to DSMC simulations (note the curvatures of the lines). Although grid adaptation is forbidden for N < 50, adaptation occurs if N = 51 which halves the particle number and increases statistical scattering in the macroscopic quantities. The profiles shown in Fig. 4 are obtained from $4 \cdot 10^4$ averages over time for each cell once steady state is reached.

To get a clearer picture we plotted in Fig. 5 the relative deviation of the simulated Ma number from the measured value on each measurement point making use of linear interpolation of simulated Ma results. The good agreement at x = 0 mm and low radii results from the inflow condition. The applied fit function does not depend on the axial distance and, hence, on profile characteristics. Moreover, the fit function covers also the values at $r/r_0 > 1$ which leads to the increased deviation at $r/r_0 <= 1$. For x = 30 mm the relative deviation is at most measurement positions quite low, especially near the center line. This we refer to the close distance to the inflow boundary. In case of x = 90 mm the relative deviation is also small, <= 10%. For larger radii the match regarding the relative deviation appears to be even better than for

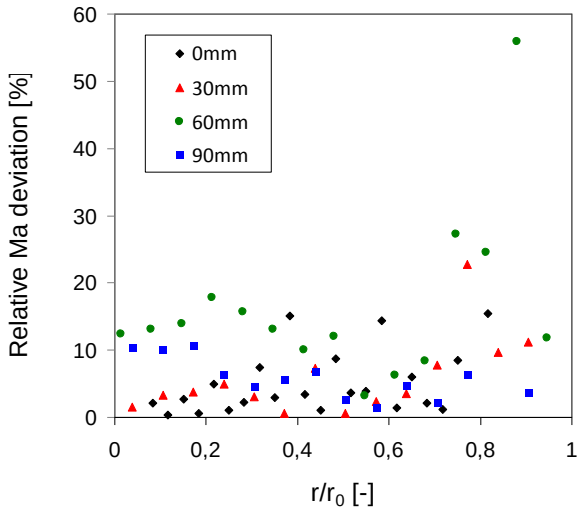

Fig. 5. Estimated deviation of Ma number between experiment and simulation.

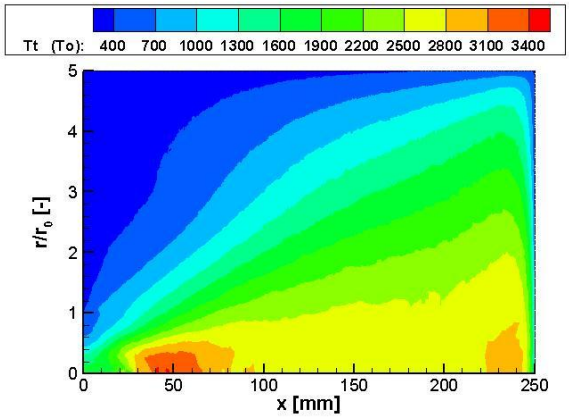

Fig. 6. Distribution of translational temperature.

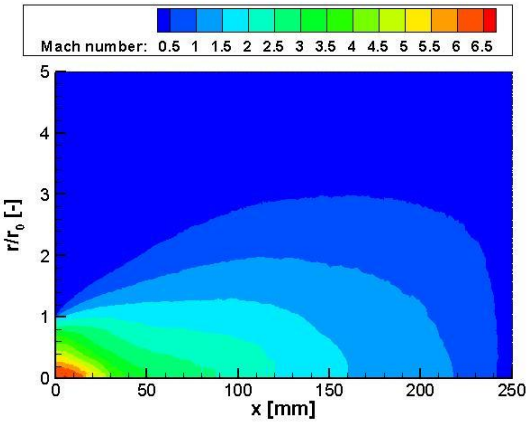

Fig. 7. Mach number distribution.

smaller radii which is contradictory to what we see at all other positions.

The largest relative deviation is observed at x = 60 mm. At most radial positions at which measurements where taken the relative deviation is > 10%, also measurement scattering is stronger than in the other cases.

Apart from the 60 mm case the relative deviation at the outer regions seem to be larger than near the center line. This is reasonable since with increasing distance from the flow center line the radial velocity component increases such that the Rayleigh-Pitot equation looses validity. Keep in mind that, strictly speaking, Rayleigh-Pitot provides accurate results if the shock front is orthogonal to the probe axis, i.e. any radial velocity components are negligible.

In Fig. 6 a temperature distribution in the whole domain is presented. A major artifact of the simulation can be observed: the influence of the fixed outflow boundary condition on the right side as well as on top. Without adaptation of the outflow boundary condition (same as tank background) the temperature at the upper and right boundary drops in an unphysical way. At the right boundary at the center line the temperature is non-physically increased due to enforced flow deceleration. Nevertheless, the *hot spot* at x = 50 mm at the center line is very typical.

But, since the right boundary is 160 mm away from the last axial measurement point the influence on the quantitative Ma number comparison is presumably very small. As can be seen in Fig. 7 the influence on the Mach number distribution is observable with respect to the curvature of the very last scale *bubble*. The Ma number distribution of the next lower scale level (at approx. at x = 200mm) shows a curvature which would be expected in case of no disturbance.

In DSMC, Δt constraints result from a) the collision frequency and the need to decouple collision and movement, and b) the analogue of the CFL condition which, however, in DSMC is not relevant for numerical stability, but for physical reality. Condition a) is realized by keeping the collision probability <1.0 which is shown in Fig. 8. The maximum collision probability in all cells and over all iteration steps never exceeds the limit. Of course, in case of high density flow simulations the physical accuracy is accompanied by a long simulation time.

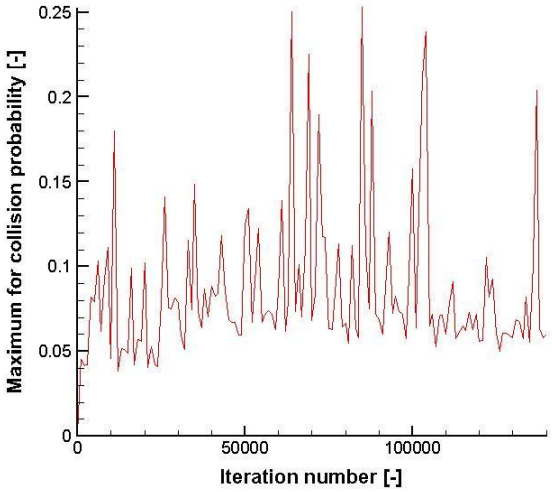

Fig. 8. History of maximum collision probability in the whole domain.

The second condition is not subject to numerical stability issues as it is in case of standard explicit continuum approaches. Instead, it has relevance for the information transport within a cell. A particle should stay long enough in a cell in order to be able to interact with other particles and, thereby, spread its own physical properties (information) throughout the cell such that a measure of macroscopic quantities reproduces well the distribution of microscopic particle properties within that cell. However, with respect to resolving the collision frequency this condition has a minor importance. Moreover, given **Fig. 8** we consider the second constraint also as fulfilled.

5. Conclusion

The newly implemented grid adaptation limitation in combination with the (also newly implemented) nearest neighbor search enables LasVegas to be applied to low Knudsen number flows. The relative deviation of about 10 % at the majority of measurement points suggests that simplifications like neglecting chemistry may have a low impact on the simulation results.

The Ma number distribution (Fig. 7) suggests a minor influence of the flow properties by the right boundary condition. However, Fig. 6 shows another picture. The fact that the non-adaptive boundary condition may influence the flow field properties downstream next to the boundary is not tolerable, the boundary model needs improvement with respect to dynamic adaptation.

The inflow condition we applied was derived in a previous work [5] and needs further verification. Given future code improvements, inflow boundary should be defined at the nozzle throat where sonic transition occurs and combustion chamber data can be used to derive accurate inflow conditions. A direct comparison of total pressure data at all axial positions would justify the derivation of a whole set of physical quantities and their radial profiles just from the total pressure measurement of high spatial resolution as a feasible way to get a broad picture of the flow properties.

Acknowlegements

The authors wish to thank the German Research Foundation and the Japan Society for the Promotion of Science for supporting this work.

References

[1]G. Herdrich, M. Fertig, S. Loehle; The Open Plasma Physics Journal, Vol. 2: 2009; pp. 150-164
[2] G. Herdrich, M. Fertig; Trans. JSASS Space Tech. Japan, Vol. 7: 2009; pp. Pe_49-Pe_58
[3] M. Laux; Doctoral thesis (in German), IRS, 1996
[4] D. Petkow, M. Fertig, G. Herdrich, M. Auweter-Kurtz; *Vacuum*, Vol. 83-1: 2008; pp. 11-14.
[5] D. Petkow G. Herdrich, D. Feldmann, M. Fertig, M. Matsui, K. Komurasaki, M. Auweter-Kurtz.; Adv. Appl. Plasma Sci., Vol. 7: 2009
[6] G. Bird; Clarendon Press, Oxford, 1994
[7] S. Nomura et al.; Paper 2008-e-30, 26th ISTS Conference, Japan, 2008
[8] G. Herdrich, D. Petkow; Journal of Plasma Physics, Vol. 74(03): 2007; pp. 391-429
[9] C. Boie; Doctoral thesis (in German), IRS, 2000
[10] M. Matsui, T. Ikemoto, H. Takayanagi, K. Komurasaki, Y. Arakawa; *J. Therm. Heat Transfer*; Vol. 21-1: 2007; pp. 247-249.